Materials Advances

ROYAL SOCIETY OF CHEMISTRY

PAPER

View Article Online
View Journal | View Issue

Cite this: *Mater. Adv.*, 2025, **6**, 5892

Oversaturated Li-FeOF solid solutions developed using LiPON interfacial coating†

Haotian Wang,[b] Binh Hoang,[a] Feng Wang,‡[c] Sz-Chian Liou,§[d] Chunsheng Wang,[e] Gary Rubloff[b] and Chuan-Fu Lin*[a]

Received 8th April 2025,
Accepted 27th June 2025

DOI: 10.1039/d5ma00338e

rsc.li/materials-advances

FeOF is a promising high-capacity cathode material for Li-ion batteries (LIBs). However, lithiation of FeOF triggers a conversion reaction once the Li content reaches approximately 0.6Li per FeOF, limiting its reversible capacity in LIB applications. Our previous work demonstrated that FeOF with LiPON coating could significantly enhance the cycling stability of FeOF electrodes (from 29% to 89% over 100 cycles). In this study, the phase transformation and phase separation of FeOF upon lithiation were tracked using (S)TEM, EELS, and *in situ* XAS under the effect of interfacial LiPON coating. We quantified that the onset potentials of the conversion reaction for LiPON-coated FeOF were delayed for ~0.3 V upon the discharged process compared with that for bare FeOF, where the thresholds of lithiation amount for the conversion reaction extends from ~0.6Li to ~1.1Li per formula unit due to the coating to form an oversaturated (supercooled) Li-FeOF solid solution. It is evidenced that the interfacial kinetics offered by the LiPON coating effectively drive the Li-FeOF system away from thermodynamic equilibrium.

Introduction

Li-ion battery technology has been very successful in utilizing the reversible process of Li-ion intercalation/deintercalation in layered cathode materials, such as $LiCoO_2$, $LiFePO_4$, and NMC, and in revolutionizing portable electronics and electric vehicles. However, the lower specific capacity of layered cathode materials has been the major bottleneck to deliver high energy density batteries. Conversion electrodes, *e.g.*, metal oxides and fluorides (such as FeF_3 and SnO_2) and alloy materials (such as Si and Sn), have drawn significant attention over the past decades as candidates for next-generation, high-capacity electrodes.[2–12] Different from the reversible redox reactions observed in layered electrode materials, the conversion reaction in these high-capacity conversion electrodes causes major chemical and structural complexities owing to the formation of new phases and interfaces that prevent the high reversibility of the conversion electrodes.

Iron fluoride (FeF_3) and iron oxyfluoride (FeOF) have been considered potentially important cathode materials for electric vehicle applications[13] as they deliver specific capacities of 712 mAh g^{-1} and 885 mAh g^{-1}, respectively.[14,15] The oxidation state of Fe^{3+} in FeF_3 and FeOF cathodes allows for intercalation and conversion storage mechanisms. During lower levels of lithiation/delithiation cycling, Li^+ ions are inserted/removed into/from the interstitial sites of structures as Fe in the lattice undergoes Fe^{3+}/Fe^{2+} redox pair transition, which makes this material an intercalation-type electrode with high reversibility. When Li^+ ion uptake exceeds a threshold, the conversion reaction occurs, causing Fe^{2+} to be reduced to Fe^0, accompanied by phase separation of Fe metal, LiF, and Li_2O. Given the chemical and structural complexities of the conversion process, the restoration to the original phases upon delithiation is hampered.[10,16]

Chevrier and Ceder *et al.* reported that in the FeOF material,[17] a conversion reaction is thermodynamically favorable, according to first-principle calculations, for a very small amount of Li concentration in FeOF. This implies that the conversion reaction takes place at the very beginning of the lithiation process, contradictory to the experimental observation that the conversion reaction occurs after reaching an intercalation of ~0.6Li per formula unit of FeOF.[18]

[a] *Department of Mechanical Engineering, The Catholic University of America, Washington, DC 20064, USA. E-mail: linc@cua.edu*
[b] *Department of Materials Science and Engineering, University of Maryland, College Park, MD 20742, USA*
[c] *Brookhaven National Laboratory, Upton, New York 11973, USA*
[d] *Maryland NanoCenter, University of Maryland, College Park, MD 20742, USA*
[e] *Department of Chemical and Biomolecular Engineering, University of Maryland, College Park, MD 20742, USA*

† Electronic supplementary information (ESI) available. See DOI: https://doi.org/10.1039/d5ma00338e

‡ Present address: Applied Materials Division, Argonne National Laboratory, Argonne, IL 60 439, USA.
§ Present address: Institute for Functional Materials and Device, Lehigh University, Bethlehem, PA 18 015, USA.

The shifted conversion reaction potential of FeOF suggests the critical role of competing kinetic effects in its lithiation pathway and has inspired a few studies to further reduce the reaction potential by modifying the surface of the FeOF cathode.[1]

Recently, we discovered that applying a ~30 nm solid electrolyte coating of lithium phosphorus oxynitride (LiPON) *via* atomic layer deposition (ALD) on FeOF electrode materials lowers the potential of the conversion reaction.[1] We found that the LiPON coating facilitates the suppression of the conversion reaction, which results in an enhanced intercalation capacity of up to ~1Li per FeOF. This conclusion was evidenced by post-mortem characterization using solid-state nuclear magnetic resonance (SS-NMR) to detect the byproduct of the conversion reaction, *i.e.*, the amount of LiF formation. At the same lithiation level, *i.e.* ~1.3Li per FeOF, LiPON-coated FeOF showed only 1/3 of the LiF formation compared with bare (un-coated) FeOF. Consequently, the suppression of the conversion reaction for LiPON-coated FeOF results in an 89% capacity retention after 100 cycles; in contrast, the bare FeOF only shows a 29% capacity retention after 100 cycles.

Other than demonstrating the long-term superior performance and electrochemical characteristics of LiPON coating FeOF from our prior publication,[1] in this work, we employed *in situ* X-ray absorption spectra (XAS) using a synchrotron X-ray light source to collect XAS to monitor the structural change in bare and LiPON-coated FeOF in real time. Results indicated that with a ~30 nm LiPON coating, the potential threshold for the conversion reaction of FeOF delayed by 0.3 V, which requires higher driving forces (larger amount of Li insertion) for the onset of conversion. Here we demonstrate that the thresholds of lithiation amount for the conversion reaction to occur can be extended from ~0.6Li to ~1.1Li per formula unit through coating to form an oversaturated (supercooled) Li-FeOF solid solution, where the interfacial kinetics offered by the LiPON coating effectively drive the Li-FeOF system away from thermodynamic equilibrium.

Result and discussion

FeOF composite electrodes are composed of FeOF nanorod-like particles with a high aspect ratio (width ~ 100 nm, length ~ 800 nm) along with binders and carbon black. Sample fabrication and preparation procedures can be found elsewhere.[1,19] Transmission electron microscopy (TEM) images of pristine FeOF and LiPON-coated FeOF particles are shown in Fig. 1(a) and (c), respectively; scanning electron microscopy (SEM) and TEM images as well as characterization data are given in Fig. S1–S3 (ESI†). The LiPON coating with a thickness of ~30 nm was applied to FeOF electrodes through atomic layer deposition (ALD).

Electrochemical evaluation

Bare FeOF and LiPON-coated FeOF are evaluated under a slow rate of the discharged (lithiation) process with a constant current density of ~50 mA g^{-1} of FeOF. The bare FeOF and LiPON-coated FeOF lithiation profiles are plotted in Fig. 1(b) and (d), respectively. In Fig. 1(b), the lithiation profile shows the conversion electrodes' characteristics, where plateaus represent the phase separation events of the conversion electrodes. The standard lithiation process of FeOF progresses through four stages given as follows:[20]

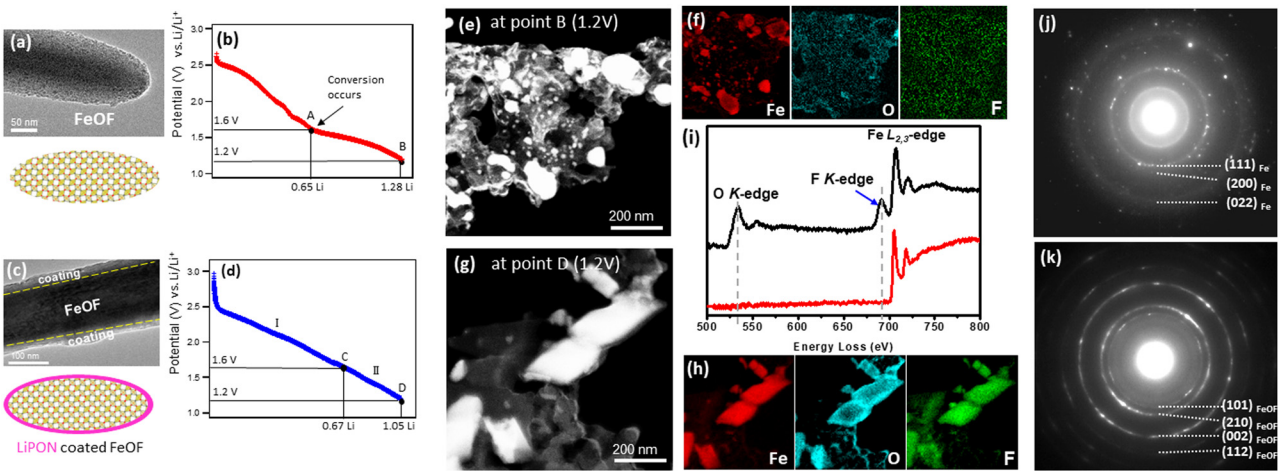

Fig. 1 (a) TEM image and the schematic of the bare FeOF particle. (b) Discharge profile of the bare FeOF electrode at 50 mA g^{-1} current density. (c) TEM image and the schematic of the LiPON-coated-FeOF particle. (d) Discharge profile of the LiPON-coated-FeOF electrode at 50 mA g^{-1} current density. (e) and (f) STEM images and EDS chemical mapping for bare FeOF after discharge to 1.2 V. (g) and (h) STEM images and EDS chemical mapping for LiPON-coated FeOF after discharge to 1.2 V; (i) EELS chemical analysis of particles in (e) – red curve and (g) – black curve; electron diffraction of bare FeOF (j) and LiPON-coated FeOF (k).

$$\underset{(rutile)}{FeOF} + Li^+ + e^- \leftrightarrow \underset{(rutile)}{Li_xFeOF} \quad eq\ 1$$

$$\underset{(rutile)}{Li_xFeOF} + (x+y-1)Li^+ + (x+y-1)e^- \leftrightarrow \underset{(rocksalt)}{Li_xFeOF_{1-y}} + yLiF \quad eq\ 2$$

$x \sim 0.6$
Conversion

$$\underset{(rocksalt)}{Li_xFeOF_{1-y}} + (1.5-x-y)Li^+ + (1.5-x-y)e^- \leftrightarrow \underset{(rocksalt)}{0.5\ Li_2FeO_2} + (1-y)LiF + 0.5\mathrm{Fe} \quad eq\ 3$$

$$\underset{(rocksalt)}{Li_2FeO_2} + 3Li^+ + 3e^- \leftrightarrow Fe + 2Li_2O \quad eq\ 4$$

The lithiation process starts with Li intercalation (eqn (1)), involving a Fe^{3+}/Fe^{2+} redox reaction without any change in the crystal structure of FeOF. Then, as the lithiation process proceeds, rutile Li_xFeOF forms a rock-salt structure, with LiF formation. At this stage, the lithiation process involves a Fe^{3+}/Fe^{2+} redox reaction, while the rutile crystal phase is transformed to a rock-salt structure (eqn (2)) till the lithium content reaches ~0.6Li, according to previous X-ray diffraction (XRD) studies.[18,21] In the next stage (eqn (3)), which is referred to as the conversion process, with lithiation greater than 0.6Li, the rock salt structure Li_xFeOF_{1-y} decomposes into Li_2FeO_2 and reduced Fe^0 transition metal. Eventually, the remaining rock salt Li_2FeO_2 gets converted into Fe metal and Li_2O (eqn (4)). The latter two processes (eqn (3) and (4)), involving the formation of Fe metal, are the main conversion reactions.

In Fig. 1(b), the discharge profile of bare FeOF showed a voltage plateau at ~1.6 V (which starts at point A in Fig. 1(b)). In contrast, the discharge profile of LiPON-coated FeOF, as shown in Fig. 1(d), did not show a similar feature—the voltage plateau is absent, suggesting that the conversion reaction is either delayed to a potential that is lower than the experimental potential limit or suppressed. The formation and separation of new phases are thermodynamically favorable but contribute to poor reversibility and large overpotentials upon charging.

We conducted the post-mortem examination of FeOF electrode discharge to 1.2 V (point B in Fig. 1(b)) by performing EELS in conjunction with scanning TEM (STEM), STEM-EELS, shown in Fig. 1(e), (f), and (i). Qualitatively, after discharge to 1.2 V, the TEM images and EELS spectra of bare FeOF not only exhibited change in morphology and dimension (Fig. 1(e) and (f)), but also revealed an absence of the O (*K*-edge at ~532 eV) and F (*K*-edge at ~685 eV) signals (Fig. 1(i)); however, the Fe signal ($L_{2,3}$ edge at ~704 eV) remained. This implied the decomposition of the FeOF electrode and the occurrence of the irreversible conversion reaction. Fig. 1(j) shows the ED pattern associated with Fig. 1(e) and reveals crystal ring patterns, indicating nano-polycrystalline particles. The calculated *d*-spacings for the rings were identified as eth Fe metal phase. (The calculated *d*-spacing data is shown in Fig. S4, ESI†) The observation from EELS elemental mapping, shown in Fig. 1(f), reveals the formation of nano-polycrystalline Fe metal particles embedded in LiF or Li_2O matrices, indicating the decomposition of the bare FeOF structure through the conversion reaction.

Surprisingly, for the lithiation of LiPON-coated FeOF, shown in Fig. 1(d), the absence of plateau suggests very limited phase transformation and separation of new phases involved during the lithium storage process. The constant slope of the discharged profile (between 2.4 V and 1.2 V) indicates a similar electrochemical behavior between lithiation processes I (between 2.4 V and 1.6 V) and II (between 1.6 V and 1.2 V). Therefore, given the absence of a plateau at point C (1.6 V) and the constant slope in the whole region of 2.4–1.2 V, it is suggested that a continuation of the Fe^{3+}/Fe_2^+ redox reaction occurred through the lithiation process beyond the previous threshold (~0.6Li) with LiPON-coated FeOF; hence, the conversion reaction was suppressed or delayed.

The STEM HAADF images, EELS elemental mapping, and extracted EELS spectrum of the LiPON-coated FeOF are shown in Fig. 1(g), (h), and (i), respectively. The corresponding EELS spectrum (black curve), in Fig. 1(i), shows the chemical composition of the LiPON-coated-FeOF electrode after discharge to 1.2 V [point D in Fig. 1(d)]. These results qualitatively show that after lithiation to 1.2 V, the chemical integrity of FeOF particles was preserved in terms of morphology (Fig. 1(g)), crystallinity (see ED pattern in Fig. 1(k)) and chemical composition (see elemental mappings in Fig. 1(h)). This is in sharp contrast to the bare FeOF—see the red curve, in Fig. 1(i), and elemental mappings, in Fig. 1(f), wherein a loss of O and F was observed. The ED pattern supports the hypothesis drawn from the electrochemical profile, the EELS spectrum, and the previously reported solid-state NMR spectra—the conversion reaction to form Fe metal from FeOF upon lithiation is suppressed or delayed in the presence of an overlayer coating of ALD LiPON.[1]

The post-mortem characterizations provide a snapshot to qualitatively understand the reaction product at a discharged potential of 1.2 V. The remaining questions that we would like to answer further are as follows: (1) with the overlayer of LiPON, is the conversion reaction fully suppressed or partially delayed? (2) Quantitatively, how much offset of conversion reaction potentials caused by the presence of the overlayer of LiPON?

In situ XANES: determination of the onset of the conversion reaction

Bare FeOF *vs.* LiPON-coated FeOF. In order to investigate the onset of the conversion reaction upon lithiation for FeOF systems with and without an overlayer, we adopted *in situ* X-ray absorption spectroscopy (XAS) measurements at the Brookhaven National Laboratory's synchrotron facility. The FeOF composite electrodes were used in *in situ* cells with 1 M $LiClO_4$ in a 1 : 1 EC : EMC liquid electrolyte. Both samples were

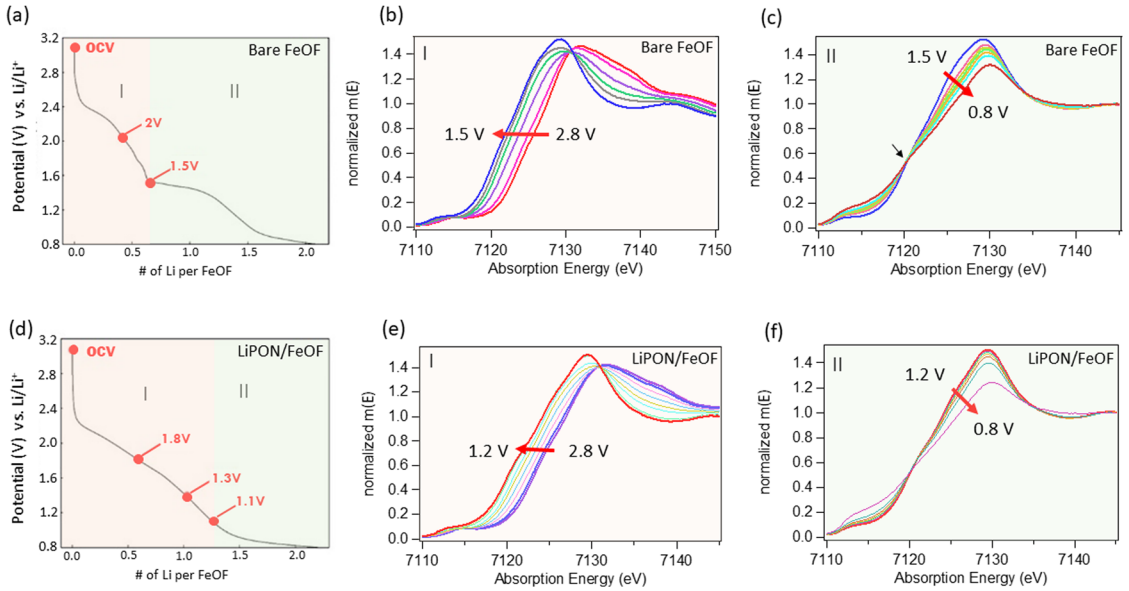

Fig. 2 (a) Discharge profile of bare FeOF; XANES spectra of bare FeOF discharged in (b) region I of 2(a) – OCV ~ 1.5 V; (c) region II (1.5–0.8 V). (d) Discharge profile of LiPON-coated FeOF; XANES spectra of LiPON-coated FeOF discharged in (e) region I of 2(d) –OCV ~1.2 V; (f) region II of 2(d) –1.2–0.8 V.

discharged at a 0.1C rate from open circuit voltage (OCV) to 0.8 V. The discharge profile of bare and LiPON-coated samples are shown in Fig. 2(a) and (d). Similar to previous electrochemistry results, bare FeOF showed a clear voltage plateau at 1.5 V, which corresponds to the conversion reaction, while LiPON-coated FeOF showed its conversion plateau at below 1.1 V. Therefore, we classify the discharge profiles into two regions: region I or "pre-conversion region" and region II or "conversion region". The voltage plateau of bare FeOF, however, is slightly lower than the previous result (1.6 V in Fig. 1(b)), possibly owing to a slightly different F/O ratio in FeOF caused by change in fabrication conditions. X-ray absorption near edge structure (XANES) spectra is obtained to track the electronic structures of and oxidation state change in Fe ions. The XANES spectra of bare and LiPON-coated FeOF at the early discharge state (process I), *i.e.*, before the onset of conversion (pre-conversion), are shown in Fig. 2(b) and (e).

In Fig. 2(b), the evolution of Fe K-edge XANES as bare FeOF discharged from 2.8 V to 1.5 V (region I) is shown. In region I, the absorption energy in Fe K-edge XANES decreases monotonically with discharged potential, which manifests a continuous reduction in the average oxidation state of Fe. The Fe^{3+} of FeOF is gradually reduced to Fe^{2+} as it undergoes the lithiation processes shown in equations 1 and 2, which is evidenced by the parallel shift in the absorption edge of the Fe K-edge XANES spectra to the lower absorption energy. Thus, in this region, the reaction is dominated by the formation of the Fe^{2+} valence state product.

In contrast, in region II, after the onset of the plateau shown in Fig. 2(a), where the discharged potential reaches 1.5 V, the characteristic of the Fe K-edge XANES spectra sharply changes. As shown in Fig. 2(c), instead of a continuous parallel edge shift, the Fe K-edge XANES spectra start to tilt and center on an isosbestic point at ~7121 eV. The presence of the isosbestic point suggests that a two-phase conversion reaction has taken place (eqn (3) and (4)),[22–24] where the reaction yields the formation of Fe^{2+} and Fe^{0} valence state products, in this region with an onset discharged potential of 1.5 V (representing >0.6Li per FeOF) for bare FeOF.

The electrochemical profile and Fe K-edge XANES spectra of LiPON-coated FeOF are shown in Fig. 2(d–f). As shown in Fig. 2, the electrochemical characteristics of LiPON-coated FeOF show two distinctive regions, (i) a nearly constant-sloped discharged profile across 2.3–1.1 V and (ii) a plateau below 1.1 V, suggesting a delayed onset of the conversion reaction compared with bare FeOF. By adopting the same criterion used to analyze bare FeOF, the *in situ* Fe K-edge XANES spectra for LiPON-coated FeOF exhibits two major trends corresponding to the two regions. In region I, as shown in Fig. 2(d), a parallel shift of Fe K-edge XANES spectra is observed with monotonically decreased absorption energy as the discharged potential reduced to 1.2 V. This indicates that LiPON-coated FeOF allows a continuous reduction from Fe^{3+} to Fe^{2+} upon Li insertion (~1Li per formula unit) without inducing a significant destruction of the structure. Below 1.2 V, an isosbestic point of Fe K-edge XANES spectra at ~7121 eV (Fig. 2(d)) suggests a major structure destruction of the FeOF crystal, and a two-phase transition occurs owing to the on-going conversion reaction. Based on the *in situ* XANES spectra, a 0.3 V delay in the onset of the conversion reaction is determined due to LiPON coating on FeOF.

Extended X-ray absorption fine structure (EXAFS) spectra: structure evolution and Fe metal formation

An extended X-ray absorption fine structure (EXAFS) was obtained to monitor the crystal structure change in FeOF during discharge.

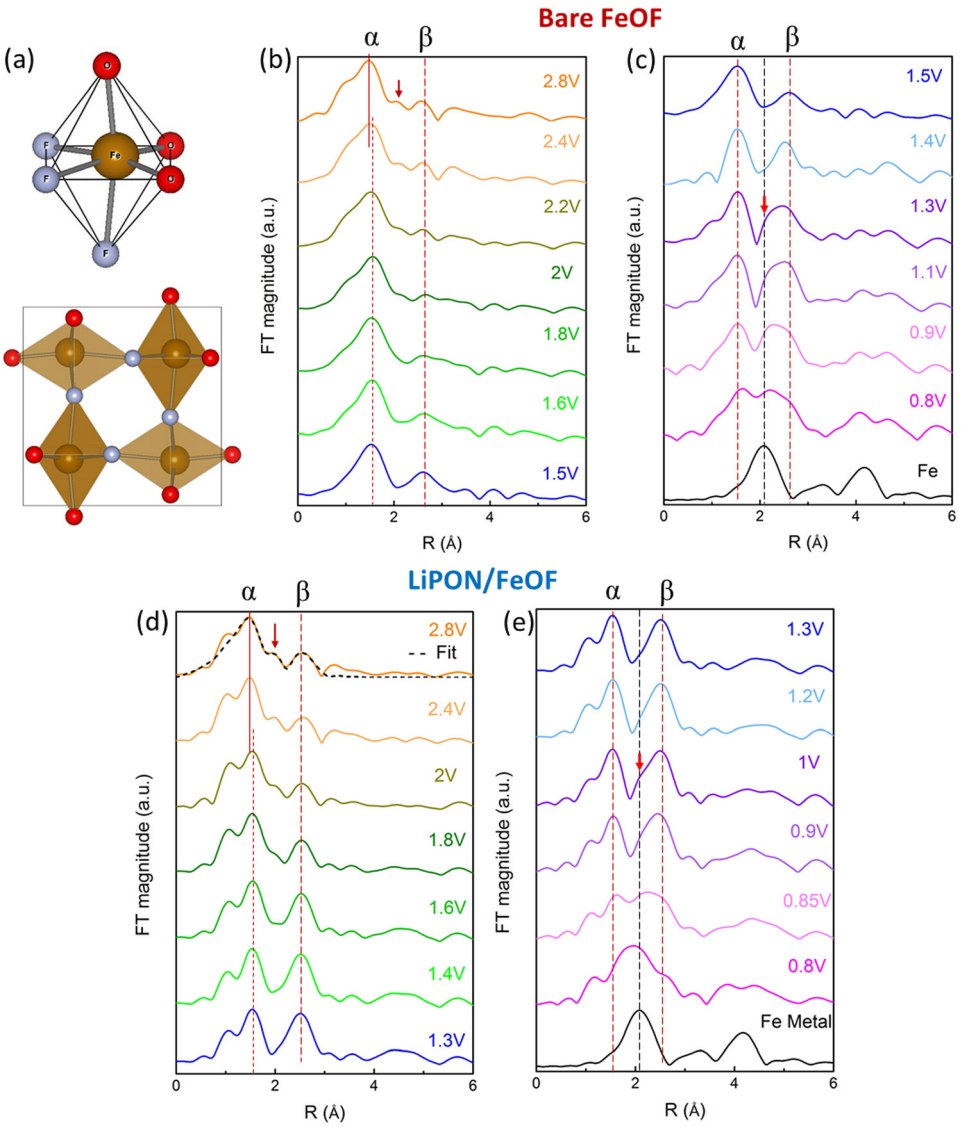

Fig. 3 (a) Crystal structure of FeOF. (Upper) Octahedral site of Fe. (Lower) Unit cell of FeOF with projection along [001], and RDF plots of (b) and (c) bare FeOF and (d) and (e) coated FeOF, where α indicates the Fe–O scattering path and β corresponds to Fe–Fe scattering of FeOF.

Additionally, radial distribution function (RDF) plots were obtained through Fourier transform of EXAFS spectra. Fitting of RDF plots was also performed to facilitate data interpretation. The model crystal structure for bare FeOF was adopted from Chevrier's work,[25] as shown in Fig. 3(a). This distorted rutile structure ($P4_2m$ space group) of FeOF was obtained from first-principles calculations using the lowest energy method. The fitting process was performed using the O–Fe, F–Fe and Fe–Fe scattering paths in the first shell, with a fitting range from 1.1 Å to 3 Å. Details of fitting parameters can be found in ESI† (Fig. S4 and Table S1). RDF plots of bare FeOF are shown in Fig. 3(b and c), with a few distinctive peaks located at 1.5 Å, 2.1 Å, and 2.6 Å. Based on the fitting result, the peaks at 1.5 Å and 2.6 Å can be assigned to the Fe–O (α) and Fe–Fe (β) scattering of FeOF in the first shell, while the shoulder peak at 2.1 Å (pointed by the red arrow in Fig. 3(b)) arises from Fe–F scattering and is not solely attributed to a single scattering path. Instead, the shoulder peak is a convolution of the Fe–F and Fe–O scattering paths. Thus, we did not assign this peak to any specific bond but used it as an indication of Fe–F bonds.

In Fig. 3(b), as bare FeOF was lithiated from 2.8 V to 2.4 V, the Fe–O bond (α) shifted to a longer distance, with the position of other bonds unchanged. This suggests the rutile structure of FeOF was distorted without significant change in the crystal structure. From 2.4 V to 1.8 V, the intensity of Fe–F gradually reduced and eventually disappeared at 1.8 V, which is explained by the loss of F atoms in FeOF and the formation of the rock-salt phase, Li_2FeO_2, in the course of lithiation (eqn (2)). The formation of LiF consumes F atoms, and rock salt Li_2FeO_2 has only one scattering path for Fe–O in the first shell, corresponding to a single peak in the range from 1.1 Å to 2.2 Å, as observed in our results. As discharge proceeds through the

conversion reaction (*i.e.*, the formation of Fe^0) from 1.5 V to 0.8 V (Fig. 3(c)), a peak at 2.06 Å emerges. This peak, based on measurement of reference Fe foil, corresponds to the Fe–Fe scattering path in BCC Fe metal. In Fig. 3(c), the magnitude of the 2.06 Å shoulder (pointed by the red arrow) increased significantly when discharging to 1.3 V, indicating the detection of Fe^0 formation in EXAFS through the conversion reaction. The intensity of the peak at 2.06 Å (Fe^0) continued to increase as it discharged to lower potentials. However, even at 0.8 V, the conversion reaction is not fully complete, where still some Fe–O (α) scattering from rock salt $LiFeO_2$ remains.

Radial distribution function (RDF) plots were also obtained from EXAFS spectra for LiPON-coated FeOF, as shown in Fig. 3(d and e). For LiPON-coated FeOF, the RDF patterns suggest different lithiation kinetics. At the beginning of discharge, the rutile phase was maintained. As the discharge process proceeded to 2 V, the extension of the Fe–O bond occurred, accompanied by a slight contraction of Fe–Fe bonding. The reason for this Fe–Fe contraction is unclear, but a possible explanation is that the mechanical confinement of the coating layer facilitated the rearrangement of Fe ions. As the voltage dropped to 1.6 V, the shoulder peak at 2.1 Å vanished, implying a transformation from a rutile to rock-salt phase. This rutile-to-rock salt transformation occurred above 1.8 V for bare FeOF, as indicated in Fig. 3(b); therefore, a 0.2–0.3 V delay in phase transformation is observed due to LiPON coating. Beyond 1.6 V, the structure of coated FeOF is mainly unchanged through 1.3 V. (Note that for bare FeOF, the formation of Fe^0 is detected at 1.3 V.)

Fig. 3(e) shows the RDF plots from 1.3 V to 0.8 V. Regarding the Fe–Fe scattering path of BCC Fe metal at 2.06 Å, LiPON-coated FeOF only started to show the formation of Fe^0 at 2.06 Å after discharge to 1.0 V (the shoulder pointed by the red arrow), indicating that the conversion reaction with Fe metal formation occurred. At the same time, rock salt $LiFeO_2$ still remained in the mixture. Compared with the case for bare FeOF (Fig. 3(c)), again a delay of ∼0.3 V for the conversion reaction (phase separation) is observed, in agreement with the XAS spectra mentioned above, which is caused by the ALD LiPON coating. However, once the voltage dropped below 0.9 V, the conversion reaction seemingly accelerated, with the product being mostly pure Fe^0 at 0.8 V. This indicates that although the conversion reaction was delayed by the LiPON coating, the formation of Fe metal was accelerated, with a higher fraction of Fe metal formed at the end of discharge compared with bare FeOF.

To summarize the effect of the LiPON coating on FeOF electrodes in terms of the Li insertion limit and the commencement of the conversion reaction, we compare the XANES and RDF plots (from EXAFS spectra) for bare and LiPON-coated FeOF, (Fig. 2 and 3). Quantitatively, the potential for the conversion reaction to take place were decreased from 1.5 V for bare FeOF to 1.2 V for coated FeOF in XANES spectra, *i.e.*, a 0.3 V delay was observed due to the coating. Similarly, the potentials for Fe^0 to be initially identified in RDF plots were shifted down from 1.3 V for bare FeOF to 1.0 V for coated FeOF, and a ∼0.3 V decrease was observed.

Electrochemically, during the continuous lithiation process, the delay in the onset potentials of the conversion reaction denotes an extended range of the Fe^{3+}/Fe^{2+} redox process, often called the intercalation process (including the rutile to rock salt phase transformation process, eqn (1) and (2)) for the coated FeOF. The downward shift in the onset potentials from 1.5 V to 1.2 V represents the intercalation limits increase from ∼0.6Li (bare FeOF, Fig. 2(a)) to ∼1.1Li per formula unit of FeOF with LiPON coating (Fig. 2(d)). Note that the lithiation limit for a Fe^{3+}/Fe^{2+} redox reaction is 1Li. Therefore, the excess lithiation (0.1Li) observed in Fig. 2(d) could be attributed to the irreversible lithium consumption in the first discharge, such as SEI formation.

LCA analysis

Furthermore, we performed linear combination fitting analysis (LCA) to estimate the relative mole fraction of different Fe oxidation states, Fe^0, Fe^{2+}, and Fe^{3+}, during lithiation. The spectra were fitted with the standards of BCC Fe metal, FeO, and Fe_2O_3, corresponding to Fe^0, Fe^{2+}, and Fe^{3+}. (See the fitting curves and *R*-values in Fig. S6 and S7, ESI†). Fig. 4(a) and (b) show the compositions as a function of discharged potential for bare FeOF and LiPON-coated FeOF, respectively. In both bare FeOF and LiPON-coated FeOF, there were already ∼10% of Fe^{2+} existed initially, which indicates that there was slightly oxygen-rich FeOF to start with, presumably caused by the electrode fabrication and processing process in the ambient environment. At higher potentials, the major reaction in lithiation was the transition from $Fe^{3+} \rightarrow Fe^{2+}$ for both cases. This is because as the lithiation process undergoes through intercalation (eqn (1)) followed by rutile → rock salt structural transformation (eqn (2)), the oxidation state of iron lowers to maintain charge neutrality. In Fig. 4(a), a noticeable amount of Fe^0 (>5%) was observed at a potential below 1.4 V, and with decreasing potential, the amount of Fe^0 increased. The formation of Fe^0 (Fe metal) originated from the conversion reaction (eqs (3) and (4)), with the excess Li^+ ions triggering phase separation to form Fe metal, LiF, and Li_2O. The LCA analysis of the formation of Fe metal agrees very well with RDF plots (EXAFS spectra) in Fig. 3. This quantitatively suggests an onset potential of 1.3 V for Fe^0 (Fe metal). The molar ratio of Fe^{3+} remained almost constant at potentials below 1.6 V; therefore, it is evidenced that the conversion reaction is mainly the transition from Fe^{2+} to Fe^0. The existence of the Fe^{3+} state of iron (a rough near-constant of 30%) at low potentials (1.3–0.8 V) is due to the non-reacted, excess FeOF in the composite electrode, residing far from the lithium ion source. According to Fig. 4(b), LiPON-coated FeOF is found to contain noticeable amounts of Fe^0 (>5%) at 1.0 V. This supports the observation shown in the RDF plots (EXAFS spectra), Fig. 3(d and e), that the Fe^0 peaks were generated at 1.0 V. Although LiPON-coated FeOF exhibits a delay in the conversion reaction, the rate of Fe^0 formation accelerates at lower potentials once Fe^0 starts to form at 0.8 V, and LiPON-coated FeOF shows ∼38% of Fe^0, compared with ∼34% Fe^0 for bare FeOF. Our understanding is that when the lithiation

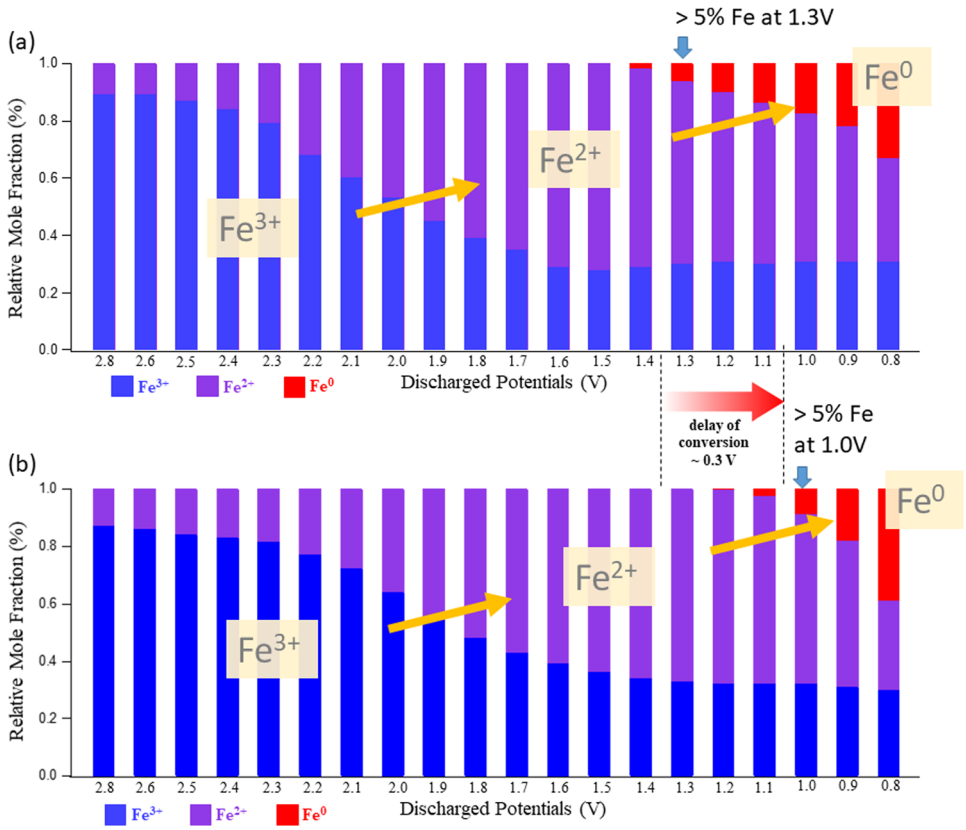

Fig. 4 Linear combination fitting analysis (LCA) for (a) bare FeOF and (b) LiPON-coated FeOF.

amount is above 0.6Li per formula unit (at/below 1.5 V), the Li/bare-FeOF solid solution is saturated, and therefore, phase separation occurs. However, the Li/coated-FeOF system forms an oversaturated (supercooled) solid solution with higher Li solubility. However, once phase separation occurs with a delay in potentials, the system quickly approaches the thermodynamic equilibrium; *i.e.*, the phase separation process (the formation of Fe^0) is accelerated.

Conclusions

In this work, we investigated the structural and chemical change in pristine FeOF and LiPON-coated FeOF using STEM-EELS and ED and quantitatively determined the onsets of the conversion reaction of pristine FeOF and LiPON-coated FeOF *via in situ* XAS. The results of STEM-EELS and ED demonstrate that LiPON-coated FeOF maintains structural integrity with lithiation amounts between 0.6 and 1.1Li per formula unit; *i.e.*, the LiPON coating facilitates the formation of oversaturated (supercooled) Li-FeOF solid solution beyond its standard threshold limit (0.6Li). XANES and EXAFS spectra show that the kinetics imposed by LiPON coating delay the onset of the conversion reaction (phase separation) of FeOF by ~0.3 V. Therefore, with the imposed kinetics by the LiPON coating, Li-FeOF solid solution demonstrates higher solubility. With higher solubility, more reversible Li (higher lithium content, *i.e.*, higher capacity) can be stored/extracted in LiPON-coated FeOF without triggering irreversible phase separation.

Experimental methods

FeOF composite electrodes

The composite electrodes of FeOF were synthesized according to a previously reported procedure.[1] The active material is composed of FeOF nanorod-like particles with a high aspect ratio—width ~100 nm and length ~800 nm (Fig. 1b–d). The thickness of the composite electrode is ~6–10 μm, with 65%–70 wt% FeOF, 20–25% carbon black, and 10% binder. The specific weight of FeOF active materials of a $\frac{1}{2}$ inch diameter electrode is in a range of 0.71–0.86 mg cm^{-2}.

ALD LiPON. We deposited ALD LiPON films in Ultratech Cambridge Nanotech Fiji F200 at 250 °C using precursors lithium *tert*-butoxide (LiO^tBu) (Aldrich, 99.7%), de-ionized H_2O, trimethylphosphate (TMP) (Aldrich, 99.9%), and N_2 gas (Praxair, grade 5.0). Argon (Airgas, grade 4.9) was used as a carrier gas. The base pressure of the ALD reactor was $<2 \times 10^{-6}$ Torr and a process pressure of 200 mTorr was maintained *via* Ar gas flow. The solid LiO^tBu precursor was kept at 165 °C and was delivered to the ALD chamber using a bubbler with 40 sccm Argon carrier gas flow. ALD films were deposited using precursor saturation doses of 3 s for LiO^tBu, 0.06 s for H_2O, and 0.4 s for TMP, and 10 s for N_2 pulse at a flow rate of 40 sccm and

a plasma power of 300 W and 30 s for Ar purge pulse. A growth rate of 1.1 Å s^{-1} was achieved for the ALD LiPON film.

Electrochemical testing. For electrochemical testing coin-type half-cells *versus* Li/Li^+ were fabricated. Lithium foil was punched to a fixed-diameter (5/8 in.) disc and was then placed on a half-inch stainless-steel disc as the current collector. Stainless-steel discs were degreased *via* sonication in a 1 : 1 mixture of isopropyl alcohol and acetone for 10 min and blow-dried using N_2. Composite FeOF electrodes were loaded into the ALD reactor for 400 ALD LiPON process cycles, which ~30 nm LiPON was deposited on the electrodes.

TEM specimen preparation

TEM lamella specimens were prepared using a focus ion beam (FIB, Tescan GAIA) and were immediately transferred into a TEM column (<5 min) to minimize any possible Li/H_2O reaction in air. Microstructure and elemental composition analyses were performed using JEOL 2100F (S)TEM equipped with a Gatan image filter (GIF, Tridiem 863). All STEM-EELS spectra were acquired at an energy resolution of 0.85 eV throughout.

In situ XAS

In situ XAS measurement was conducted at beamline 7, NSLS-II, BNL. *In situ* coin cells with view windows made of Kapton on both sides were used during the characterization. Energy calibration was performed first using a standard Fe foil. The first inflection point in the Fe XAS spectrum was calibrated to 7112 eV as the 1s–3d absorption edge of metallic Fe. Standard reference spectra from FeO_2, Fe_2O_3, and Fe powders were collected for composition analysis and Fe oxidation state analysis. During XAS acquisition of FeOF samples (bare FeOF and LiPON/FeOF), Fe-K edge spectra were recorded every 13 minutes, corresponding to an average of +0.05 state of lithiation per spectrum. IFEFFIT-Athena was used for XAS data processing and analysis.[26]

EXAFS/RDF analysis

EXAFS spectra were processed using the Athena program.[26] Polynomials were fitted to the pre-edge and post-edge and subtracted from the data. Then, the relative modulation of the absorption coefficient above the Fe K-edge was fit with a smooth spline, which represents a single Fe atom absorption pattern. The spline was subsequently subtracted, and the remaining spectrum was normalized using a theoretically calculated u_0 value. k-weight = 2 was used to equally emphasize the modulation in low and high wavenumber ranges. Thereafter, EXAFS spectra from k = 3−11 and $R_{bkg} > 1$ were Fourier transformed to generate RDF patterns. The fitting process was conducted using the Artemis program.[26] The model crystal structure and the accompanied scattering paths were generated based on the *ab initio* program FeFF8.[27] In order to minimize the correlation between fitting parameters and reduce the total number of floating parameters, the fitting was first performed on a model material, as-fabricated pristine FeOF. The single values of the amplitude reduction factor (S_0^2) and energy shift (ΔE_0) are obtained and used for following fittings. The fitting was then performed on bare and coated FeOF samples.

Conflicts of interest

The authors declare no competing financial interests.

Data availability

The data supporting the findings of this study are comprehensively detailed within the main manuscript, which includes all critical figures and experimental results such as high-resolution TEM images, EELS spectra, EDS mappings, XANES spectra, RDP plots, and LCA data. Additional supporting data, including extended analyses, supplementary figures, and detailed experimental procedures, are available in the ESI† accompanying this article. ESI† provides in-depth methodological details, including the high-resolution TEM images of LiPON-coated FeOF, ToF-SIMS spectra, TEM tomography of composite FeOF, EXAFS spectra, and XAFS fitting involved in the study. Owing to confidentiality and intellectual property considerations, certain raw data, including proprietary synthesis protocols and specific experimental details, cannot be publicly disclosed. However, processed data, which have been rigorously analyzed and are essential for reproducing the findings of this study, are available upon reasonable requests. Interested researchers should contact the corresponding author, Dr Chuan-Fu Lin, to discuss data access and any necessary agreements to ensure appropriate use and protection of the information.

Acknowledgements

This work was supported by the U.S. Department of Energy, Office of Science, Office of Basic Energy Sciences, under Award Number DE-SC0024274. The authors would like to acknowledge Prof. Yue Qi and Dr Qisheng Wu from Brown University for the fruitful discussion on the crystal structures of FeOF under phase transformation. We acknowledge the support of the AIM Lab, in Maryland NanoCenter at University of Maryland, College Park.

References

1 C. F. Lin, X. Fan, A. Pearse, S. C. Liou, K. Gregorczyk, M. Leskes, C. Wang, S. B. Lee, G. W. Rubloff and M. Noked, Highly Reversible Conversion-Type FeOF Composite Electrode with Extended Lithium Insertion by Atomic Layer Deposition LiPON Protection, *Chem. Mater.*, 2017, **29**(20), 8780–8791, DOI: 10.1021/acs.chemmater.7b03058.

2 J. Mavračić, F. C. Mocanu, V. L. Deringer, G. Csányi and S. R. Elliott, Similarity between Amorphous and Crystalline Phases: The Case of TiO_2. Journal of Physical, *Chem. Lett.*, 2018, **9**(11), 2985–2990, DOI: 10.1021/acs.jpclett.8b01067.

3 O. Delmer, P. Balaya, L. Kienle and J. Maier, Enhanced Potential of Amorphous Electrode Materials: Case Study of

RuO_2, *Adv. Mater.*, 2008, **20**(3), 501–505, DOI: **10.1002/adma.200701349**.

4 F. Wang, R. Robert, N. A. Chernova, N. Pereira, F. Omenya, F. Badway, X. Hua, M. Ruotolo, R. Zhang, L. Wu, V. Volkov, D. Su, B. Key, M. Stanley Whittingham, C. P. Grey, G. G. Amatucci, Y. Zhu and J. Graetz, Conversion Reaction Mechanisms in Lithium Ion Batteries: Study of the Binary Metal Fluoride Electrodes, *J. Am. Chem. Soc.*, 2011, **133**(46), 18828–18836, DOI: **10.1021/ja206268a**.

5 G. Jain, J. Yang, M. Balasubramanian and J. J. Xu, Synthesis, Electrochemistry, and Structural Studies of Lithium Intercalation of a Nanocrystalline Li_2MnO_3-like Compound, *Chem. Mater.*, 2005, **17**(15), 3850–3860, DOI: **10.1021/cm0503329**.

6 G. Jain, M. Balasubramanian and J. J. Xu, Structural Studies of Lithium Intercalation in a Nanocrystalline α-Fe_2O_3 Compound, *Chem. Mater.*, 2006, **18**(2), 423–434, DOI: **10.1021/cm052014f**.

7 X. Hua, R. Robert, L. S. Du, K. M. Wiaderek, M. Leskes, K. W. Chapman, P. J. Chupas and C. P. Grey, Comprehensive Study of the CuF_2 Conversion Reaction Mechanism in a Lithium Ion Battery, *J. Phys. Chem. C*, 2014, **118**(28), 15169–15184, DOI: **10.1021/jp503902z**.

8 Z. Fan, W.-R. Liu, L. Sun, A. Nishio, R. Szczęsny, Y.-G. Lin, S. Okada and D. H. Gregory, Carbon-Free Conversion of SiO_2 to Si via Ultra-Rapid Alloy Formation: Toward the Sustainable Fabrication of Nanoporous Si for Lithium-Ion Batteries, *ACS Appl. Mater. Interfaces*, 2023, **15**(30), 36076–36085, DOI: **10.1021/acsami.3c02197**.

9 J. Yoo, J. Kim, M. Choi, Y. Park, J. Hong, K. M. Baek, K. Kang and Y. S. Jung, Extremely High Yield Conversion from Low-Cost Sand to High-Capacity Si Electrodes for Li-Ion Batteries, *Adv. Energy Mater.*, 2014, **4**(16), 1400622, DOI: **10.1002/aenm.201400622**.

10 J. Li, S. Hwang, F. Guo, S. Li, Z. Chen, R. Kou, K. Sun, C.-J. Sun, H. Gan, A. Yu, E. A. Stach, H. Zhou and D. Su, Phase Evolution of Conversion-Type Electrode for Lithium Ion Batteries, *Nat. Commun.*, 2019, **10**(1), 2224, DOI: **10.1038/s41467-019-09931-2**.

11 F. Proietto, R. Rinicella, A. Galia and O. Scialdone, Electrochemical Conversion of CO_2 to Formic Acid Using a Sn Based Cathode: Combined Effect of Temperature and Pressure, *J. CO_2 Util.*, 2023, **67**, 102338, DOI: **10.1016/j.jcou.2022.102338**.

12 B. Hoang, V. Castagna Ferrari, H. Wang, D. M. Stewart, R. Damircheli and C. F. Lin, From Amorphous to Crystalline Thin-Film FeF_3 Conversion Electrodes by Sputtering Deposition, *ACS Appl. Energy Mater.*, 2023, **6**(19), 10005–10011, DOI: **10.1021/acsaem.3c01593**.

13 D. Andre, S. J. Kim, P. Lamp, S. F. Lux, F. Maglia, O. Paschos and B. Stiaszny, Future Generations of Cathode Materials: An Automotive Industry Perspective, *J. Mater. Chem. A*, 2015, 6709–6732, DOI: **10.1039/c5ta00361j**.

14 G. G. Amatucci, N. Pereira, F. Badway, M. Sina, F. Cosandey, M. Ruotolo and C. Cao, Formation of Lithium Fluoride/Metal Nanocomposites for Energy Storage through Solid State Reduction of Metal Fluorides, *J. Fluor. Chem.*, 2011, **132**(12), 1086–1094, DOI: **10.1016/j.jfluchem.2011.06.033**.

15 H. Li, P. Balaya and J. Maier, Li-Storage via Heterogeneous Reaction in Selected Binary Metal Fluorides and Oxides, *J. Electrochem. Soc.*, 2004, **151**(11), A1878, DOI: **10.1149/1.1801451**.

16 R. Porhiel, S. Belin, F. Alloin, C. Iojoiu and K. Guérin, Temperature Driven Phase Evolution of FeF_3 as Active Material in Lithium-Ion Batteries, *ACS Appl. Energy Mater.*, 2024, **7**(15), 6437–6446, DOI: **10.1021/acsaem.4c01129**.

17 V. L. Chevrier, G. Hautier, S. P. Ong, R. E. Doe and G. Ceder, First-Principles Study of Iron Oxyfluorides and Lithiation of FeOF, *Phys. Rev. B: Condens. Matter Mater. Phys.*, 2013, **87**(9), 094118, DOI: **10.1103/PhysRevB.87.094118**.

18 K. M. Wiaderek, O. J. Borkiewicz, E. Castillo-Martínez, R. Robert, N. Pereira, G. G. Amatucci, C. P. Grey, P. J. Chupas and K. W. Chapman, Comprehensive Insights into the Structural and Chemical Changes in Mixed-Anion FeOF Electrodes by Using Operando PDF and NMR Spectroscopy, *J. Am. Chem. Soc.*, 2013, **135**(10), 4070–4078, DOI: **10.1021/ja400229v**.

19 X. Fan, C. Luo, J. Lamb, Y. Zhu, K. Xu and C. Wang, PEDOT Encapsulated FeOF Nanorod Cathodes for High Energy Lithium-Ion Batteries, *Nano Lett.*, 2015, **15**(11), 7650–7656, DOI: **10.1021/acs.nanolett.5b03601**.

20 X. Fan, E. Hu, X. Ji, Y. Zhu, F. Han, S. Hwang, J. Liu, S. Bak, Z. Ma, T. Gao, S. C. Liou, J. Bai, X. Q. Yang, Y. Mo, K. Xu, D. Su and C. Wang, High Energy-Density and Reversibility of Iron Fluoride Cathode Enabled via an Intercalation-Extrusion Reaction, *Nat. Commun.*, 2018, **9**(1), 2324, DOI: **10.1038/s41467-018-04476-2**.

21 M. Sina, N. Pereira, G. Amatucci and D. Sue, Structural Transformations Of FeOF/C Nanocomposite Electrodes Upon Charging/Discharging In Li-Ion Batteries, *Microsc. Microanal.*, 2012, **18**(S2), 1412–1413, DOI: **10.1017/S1431927612008914**.

22 T. Nowicka-Jankowska, *Some Properties Of Isosbestic Points*, Pergamon Press, 1971, vol. 33, pp. 2043–2050.

23 M. D. Cohen and E. Fischer, *588. Isosbestic Points*, 1937, 3044–3052.

24 F. Wang, S. W. Kim, D. H. Seo, K. Kang, L. Wang, D. Su, J. J. Vajo, J. Wang and J. Graetz, Ternary Metal Fluorides as High-Energy Cathodes with Low Cycling Hysteresis, *Nat. Commun.*, 2015, **6**, 6668, DOI: **10.1038/ncomms7668**.

25 V. L. Chevrier, G. Hautier, S. P. Ong, R. E. Doe and G. Ceder, First-Principles Study of Iron Oxyfluorides and Lithiation of FeOF, *Phys. Rev. B: Condens. Matter Mater. Phys.*, 2013, **87**(9), 094118, DOI: **10.1103/PhysRevB.87.094118**.

26 B. Ravel and M. Newville, Athena, Artemis, Hephaestus: Data Analysis for X-Ray Absorption Spectroscopy Using Ifeffit, *J. Synchrotron Radiat.*, 2005, **12**(4), 537–541, DOI: **10.1107/S0909049505012719**.

27 J. J. Rehr, R. C. Albers and S. I. Zabinsky, High-Order Multiple-Scattering Calculations of x-Ray-Absorption Fine Structure, *Phys. Rev. Lett.*, 1992, **69**(23), 3397–3400, DOI: **10.1103/PhysRevLett.69.3397**.